*energies*

MDPI

*Article*

# Structural Performance-Based Design Optimisation of a Secondary Mirror for a Concentrated Solar Power (CSP) Plant

**Lucio Pinello [1], Massimo Fossati [1], Marco Giglio [1], Francesco Cadini [1,*], Carla Bevilacqua [2], Mario Cilento [2], Fulvio Bassetti [2] and Raffaello Magaldi [2]**

[1] Department of Mechanical Engineering—Politecnico di Milano, Via La Masa 1, 20156 Milano, Italy; lucio.pinello@polimi.it (L.P.); massimo.fossati@polimi.it (M.F.); marco.giglio@polimi.it (M.G.)
[2] Magaldi Power S.p.A., Piazza di Pietra 26, 00186 Roma, Italy; carla.bevilacqua@magaldi.com (C.B.); mario.cilento@magaldi.com (M.C.); fulvio.bassetti@magaldi.com (F.B.); raffaello.magaldi@magaldi.com (R.M.)
* Correspondence: francesco.cadini@polimi.it

**Abstract:** Concentrated Solar Power (CSP) plants use mirrors to reflect and concentrate sunlight onto a receiver, to heat a fluid and store thermal energy, at high temperature and energy density, to produce dispatchable heat and/or electricity. The secondary mirror is a critical component in the optical system of certain Solar Power Tower plants (SPT), as it redirects the concentrated sunlight from the primary mirror onto the receiver, which can be arranged at ground level. In this study, we propose a design optimisation for the secondary mirror of a CSP plant. The design optimisation method consists of two steps. The first step involves the use of the finite element simulation software Abaqus 2022 to analyse the structural performance of the secondary mirror under thermal loads and wind. The second step consists of the use of simulation results to identify the combination of design parameters and best performances, with respect to both design constraints and structural safety. This is carried out by developing an algorithm that selects those configurations which satisfy the constraints by using safety coefficients. The proposed optimisation method is applied to the design of a potential configuration of a secondary mirror for the beam-down of the CSP Magaldi STEM® technology, although the methodology can be extended to other components of CSP plants, such as primary mirrors and receivers, to further enhance the structural performance of these systems.

**Keywords:** optimisation; design optimisation; structural optimisation; CSP plant; secondary mirror; secondary mirror optimisation; renewable energies



**Citation:** Pinello, L.; Fossati, M.; Giglio, M.; Cadini, F.; Bevilacqua, C.; Cilento, M.; Bassetti, F.; Magaldi, R. Structural Performance-Based Design Optimisation of a Secondary Mirror for a Concentrated Solar Power (CSP) Plant. *Energies* **2023**, *16*, 6000. https://doi.org/10.3390/en16166000

Academic Editors: Tariq Kamal and Syed Zulqadar Hassan

Received: 14 July 2023
Revised: 14 August 2023
Accepted: 14 August 2023
Published: 16 August 2023



## 1. Introduction

In recent years, concern about renewable energies increased due to the emissions caused by fossil fuels, and their impact on pollution and global warming. Forty per cent of the energy coming from fossil fuels is used for cooling, heating, and air conditioning in buildings [1,2]. Among renewable energies, special attention is paid to solar energy and in particular to the Concentrating Solar Power (CSP) systems which represent one of the most promising technologies to take advantage of solar energy. Among them, the Solar Power Tower (SPT) uses mirrors to concentrate direct sunlight in a focal point, obtaining intensive and highly variable direct solar power fluxes, that are transferred to a heat transfer fluid [3,4]. Heat storage systems integrated into CSP plants allow for generating heat and/or electricity not only during sunny hours but on demand. To achieve the high temperatures required for steam generation, the solar radiation must be concentrated using effective methods, based on accurate design and fabrications. A proper design is fundamental since it has been found that heliostats and receivers produce the largest exergy loss in these plants [2,5]. Thus, the technological challenge in the solar field is to ensure the required optical precision, efficiency, and robustness against environmental influences, such as wind and temperature fluctuations, at the lowest possible cost [6].

Among the SPT configurations, beam-down technology is currently attracting increasing interest worldwide: the sunrays reflected by the heliostat field point to a secondary mirror, that reconcentrates the solar radiation into the receiver, which is placed on the ground rather than on top of the tower. The beam-down technology allows for obtaining greater concentrations of sunlight and helps reduce maintenance and operating costs, compared to solar applications where reacting solids are involved or heavy equipment must be placed on top of conventional towers [7]. Beam-down installations have been realised in Japan, Israel, United Arab Emirates, China, and Italy [8]. The beam-down optical experiment [9,10] (BDOE) at the Khalifa University's Masdar Institute Solar Platform (Abu Dhabi, UAE) and Magaldi STEM® [11], developed by Magaldi Power (Italy), are recent examples of CSP plants implemented with beam-down concentrators.

### *1.1. Magaldi STEM® Description*

Magaldi STEM® system represents a technological breakthrough in the solar energy sector, as it is the only CSP technology that uses a fluidised bed of solid particles for both the solar receiver and thermal energy storage system, with completely recyclable and eco-compatible components. Magaldi technology is based on one or more modules, each of them composed of the following main subsystems:

- One heliostat field with motorised mirrors tracking the sun's position.
- A beam-down tower with secondary mirrors.
- A fluidised bed solar receiver with an integrated thermal energy storage (TES) system constituted of silica sand, which is stable to temperatures beyond 1000 °C, enabling energy storage as sensible heat with large energy density.
- A fluidising gas supply system, including air distribution manifolds, blower, air preheater, filter unit, and induced draft fan.
- A feedwater/steam circuit, including once-through in-bed heat exchangers, condenser, deaerator, and feeding pump, to produce dispatchable heat and/or electricity.
- Control systems for heliostat sun tracking and fluidised bed receiver operations.

Two prototypes of different dimensions have been built and tested. A 200 kW thermal pilot prototype was installed in Magaldi's factory (Buccino, Italy) in 2012. The second facility is a 2 MW thermal scaled-up prototype in San Filippo del Mela (Messina, Italy) which has been operating since July 2016 for over 12,000 h of extensive testing. The fluidised bed has been heated up to over 600 °C and operated in a typical range of temperature of 300–600 °C. Figure 1 shows a picture of the Magaldi STEM® prototype plant.

**Figure 1.** Magaldi STEM® pilot plant in San Filippo del Mela, Italy.

### *1.2. Beam-Down Mirror DESIGN and Optimisation*

The thermal and mechanical design [7] of secondary mirrors is a critical topic in the optical system of beam-down plants. The main challenges for such mirror design are its high operating temperature, high shape accuracy, and high reflectivity. Mirror severe temperatures evolve mainly due to the amount of irradiance that is being absorbed by the mirror and, to a lesser extent, due to convective heat exchange with the environment. Exposure to high flux densities originating from the primary concentration field, part of which is absorbed by the mirror, heats the secondary mirror with daily cycles. Hence, the mirrors are exposed to environmental conditions such as humidity and dust, high radiation fluxes, and elevated temperatures; therefore, they are subjected to thermal stresses, deformations, and degradation throughout time. For most solar reflectors, exposure during service to sunlight, particularly to ultraviolet wavelengths, high temperatures, and moisture, can lead to a loss in reflectance that would lead to higher absorbed flux [12], and thus to secondary mirror overheating. This, in turn, may lead to large deformations and poor shape quality or even mirror damage. Several works provide a comprehensive overview of the available different secondary reflector materials and different CSP configurations, which confirms the importance of analysing secondary concentrators, by simulating [7] and testing [3,7] relevant operating conditions. Having a robust thermal–structural design workflow allows the secondary reflector mirrors to withstand a higher concentration ratio at the secondary reflector, i.e., the ratio between areas of primary and secondary mirrors. This helps to improve plant competitiveness and decrease the levelised cost of heat (LCOH), as a consequence of the reduction in overall beam-down tower dimensions and shadowing losses. The literature focused on plant layout and receiver dimension optimisation by minimising the LCOE or maximising the efficiency of the plants [13,14]. Other works focused on fluidisation technologies [15] or materials for fluidised beds [9,16] for beam-down CSP plants. Studies on CSP plants' exergy analysis are present [2,5], highlighting that heliostats and central receivers are the major sources of exergy loss. However, little attention seems to have been paid to the structural design of the secondary mirrors. In this context, the authors investigated the optimisation of the design of a secondary mirror substrate consisting of a stainless steel plate with a highly reflective mirror layer, with an expected reflectance greater than 90%, considering that all the secondary mirrors share the same design regardless of their arrangement, which, therefore, is not studied in this work. The investigations aim to define the secondary mirror-optimised structural design, to withstand thermo-mechanical stresses, working with daily thermal cycles. This work is part of the Research and Innovation Project "SOLARGRID: Sistemi sOlari termodinamici e fotovoLtaici con Accumulo peR co-GeneRazIone e flessibilità Di rete", jointly funded by the European Union and Italian Research and University Ministry (MIUR). The SOLARGRID project plans to develop innovative and improved solutions for systems and components related to Concentrated Solar Power (CSP) and Concentrated PhotoVoltaics (CPV) technologies, to enhance their energetic performances and economic competitiveness in applications for distributed generation of both electric and thermal energy.

## 2. Methodology

This section focuses on the methodology employed for the development of this study. It consists of three subsections: the description (i) of the base design, (ii) of the developed structural model under optimisation, and (iii) of the algorithms. The structural model under analysis is developed in Abaqus and Python code is implemented which modifies the structural model according to the different configurations and lets Abaqus run the FEM analysis. Eventually, the Python code stores, for each configuration, the results of the analysis that are going to be used in the optimisation algorithm implemented in MATLAB. Figure 2 summarises the approach used in this study.

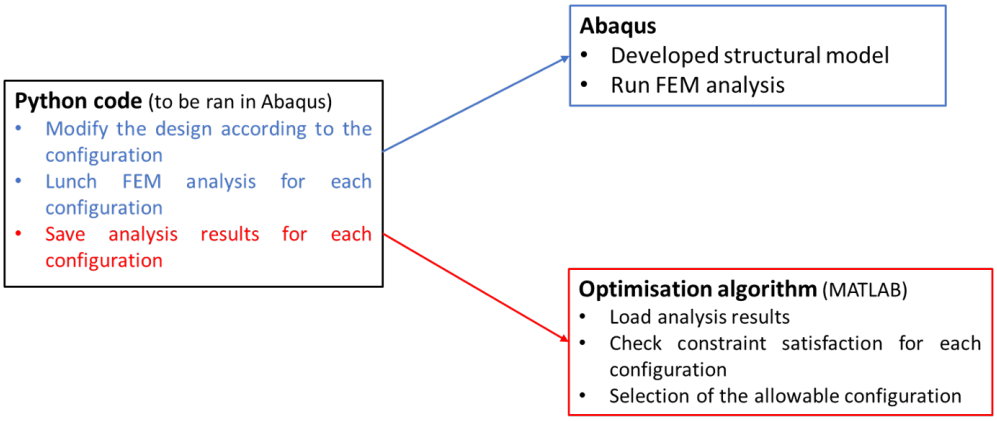


**Figure 2.** Scheme of the approach used for performing the structural design optimisation.

### *2.1. Base Design*

The base design of the secondary mirror consists of a stainless steel plate with 5 mm thickness with one reflective side with an assumed solar-weighted reflectivity of about 90%, acting as a mirror. On the other side, there are brackets for mounting the secondary mirror on its support. The mirror is shown in Figure 3. The secondary mirrors are assumed to be placed at 12 m height and oriented at 13.5° with respect to the horizontal, as shown in Figure 3. The mirrors are subjected to their weight and to the environmental and operational conditions, that are the wind and the temperature. The temperature acts as a daily thermal cycle of 200 °C, while the foreseen wind speeds are 45 m/s for 3 s gusts at 10 m above the ground and 30 m/s (10 min temporal mean) at 10 m above the ground, as reported in Table 1.

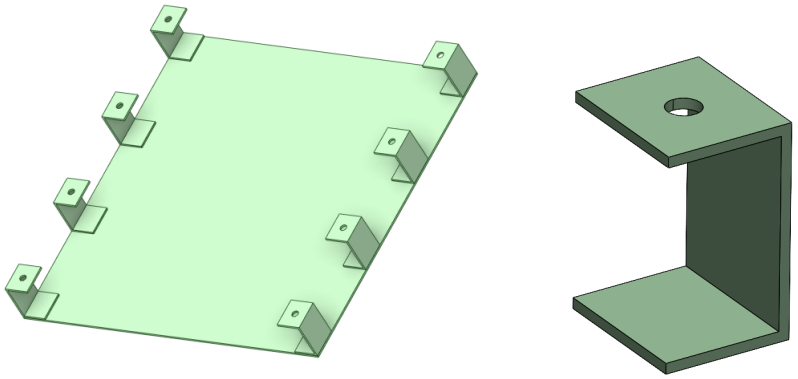

**Figure 3.** Original design of the secondary mirror on the left and focus on the bracket on the right.

**Table 1.** Foreseen wind speed.

| Parameter | Value |
|---|---|
| Basic wind speed (3 s gust) at 10 m above ground ($v_b$) | 45 m/s |
| Basic wind speed (10 min mean) at 10 m above ground ($v_b$) | 30 m/s |

### *2.2. Developed Structural Model*

The structural model under optimisation is developed in Abaqus. The plate and the brackets have been modelled as 2D shell planar thanks to the intrinsic slenderness of these structures, allowing for computational advantages in terms of both costs and time. The plate dimensions have been assumed to be 800 × 800 mm, as reported in Figure 4, while the plate thickness is one of the parameters under optimisation and is supposed to vary between 1 mm and 5 mm with increments of 1 mm. These values have been selected to

reduce the weight and cost of the mirrors with respect to the base design presented in the previous section while holding the same plate surface. The brackets are C-shaped, as shown in Figure 5, and their height varies from 80 mm to 200 mm with increments of 20 mm. The bracket thickness varies similarly to the plate one, i.e., from 1 mm to 5 mm with steps of 1 mm. The brackets' thickness is designed to vary together with the plate one for manufacturing reasons since in this way it is possible to avoid welding together components with too different thicknesses. The lower limit of the brackets' height is imposed to give the structure enough flexibility to deform without excessive rises in the stress state under the loads, while the higher one is set to limit the deformation of the mirror to minimise optic losses, the weight, and cost of the structure. The width of the bracket is constant and equal to 50 mm, in the plane perpendicular to Figure 5. The number of brackets can vary, allowing for choosing the best configuration available. Referring to Figure 6, the bracket number (#C) can vary from 6 to 9 where:

- If $\#C = 6$, the highlighted brackets are excluded from the configuration.
- If $\#C = 7$, the highlighted central bracket is included in the configuration.
- If $\#C = 8$, only the highlighted central bracket is excluded from the configuration.
- If $\#C = 9$, all the brackets are included in the configuration.

The brackets are connected to the plate using the tie kinematic contact by choosing the plate as the master element and four points of the bracket as the slave elements, as depicted in Figure 7, to represent the welding of the bracket on the plate. This contact type allows for the computation of the reaction forces at the welds and, thus, for performance of the safety assessment at the weld.

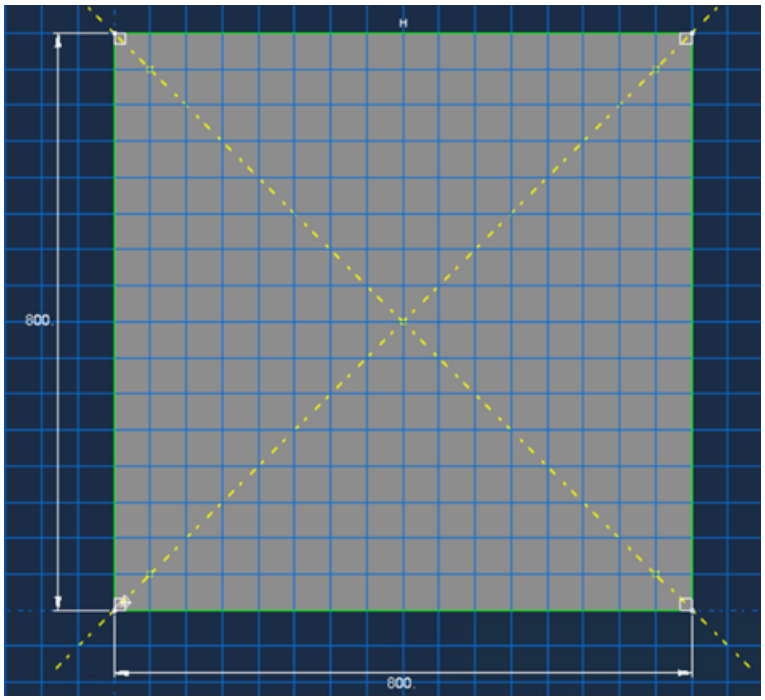


**Figure 4.** Sketch of the base secondary mirror; units are in mm.

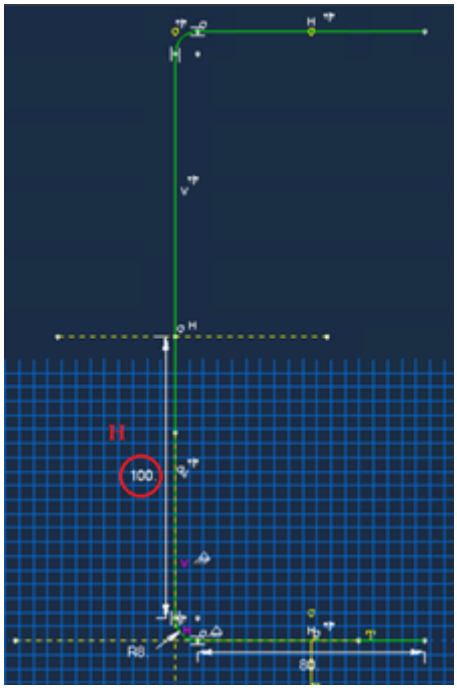


**Figure 5.** Sketch of the base secondary mirror bracket; units are in mm.

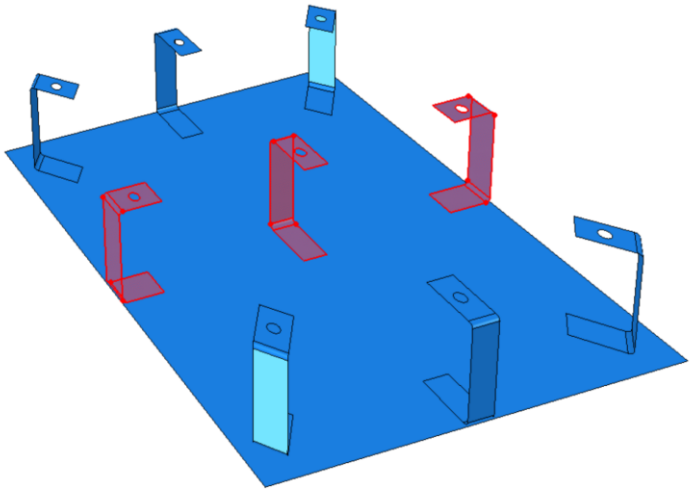

**Figure 6.** Assembly of the C-shaped brackets on the plate. The brackets in red are the ones which are included or excluded from the analysis depending on the configuration.

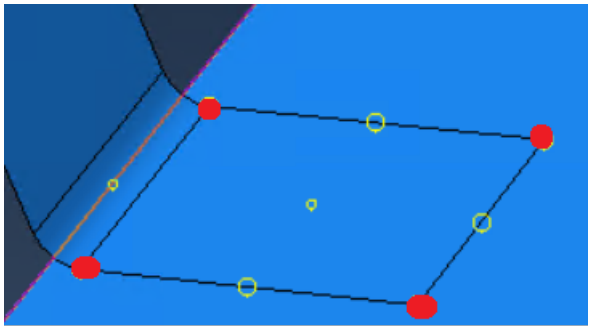

**Figure 7.** Tie contact modelling between plate and brackets.

To resume, 4 parameters are under optimisation: plate thickness, bracket number, height, and thickness, as reported in Table 2, for a total of 700 possible configurations. To

evaluate the structural performances of each configuration, suitable loads are applied to the structure; in particular, other than the gravity, the design includes the following:

- The thermal load is applied by imposing a homogeneous temperature of 200 °C to both plate and brackets.
- The wind load is applied as the drag and lift pressures acting on the plate surface in two different wind conditions:
  - Mean wind, with a speed of 13 km/h.
  - Maximum wind, with a speed of 30 m/s.

The loads are applied singularly to observe the effects of each condition on the structure. The number and location of the brackets under optimisation are based on the deformation of the plate caused by the thermal expansion: due to the imposed uniform temperature on the plate, the latter will expand uniformly along the two dimensions. Therefore, the brackets are placed symmetrically with respect to the vertical axis of the plate passing through its centre (the same hold for the horizontal axis since the plate is a square). The central bracket is added to increase the stiffness of the mirror in the central region.

**Table 2.** Parameters under optimisation.

| | *#C* | Bracket Thickness [mm] | Bracket Height [mm] | Plate Thickness [mm] |
|---|---|---|---|---|
| min | 6 | 1 | 80 | 1 |
| max | 9 | 5 | 200 | 5 |
| step | 1 | 1 | 20 | 1 |

To perform the analysis automatically in each configuration, Python code has been used that loads the Abaqus CAE model and varies the parameters, performing simulations. The number of brackets changes by activating and deactivating the contact according to the configuration. The meshed assembly is shown in Figure 8.

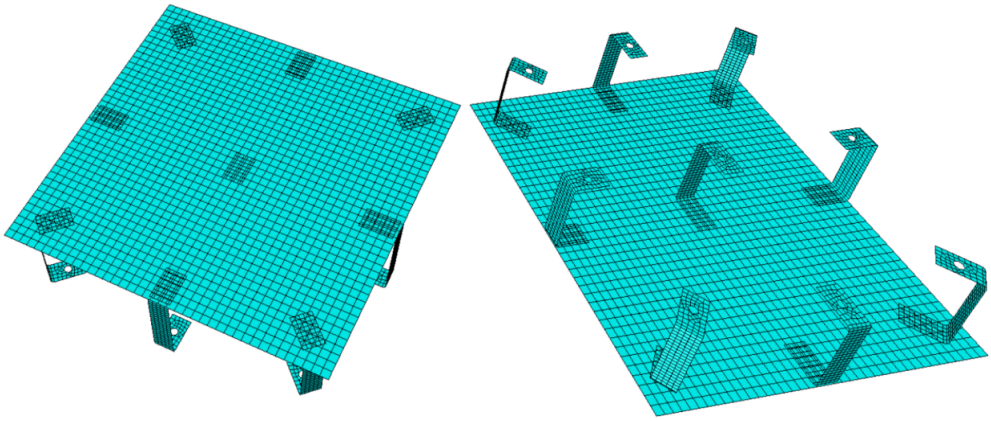

**Figure 8.** Meshed assembly.

### *2.3. Algorithm*

A Matlab algorithm is implemented to analyse the results in each configuration. The use of algorithms for data processing while respecting constraints represents a consolidated practice in the field of engineering. Specifically, within the scope of structural engineering, this class of algorithms is typically employed to guide the design of a structure towards the optimisation of certain desired properties, such as minimising its weight and/or maximising its stiffness (thus minimising the expected deformation when the structure is subjected to predetermined loads). In this context, integrating the design phase of the secondary mirror structure with optimisation algorithms represents a valid alternative to achieve optimal design conditions. In the specific case of the SOLARGRID research project,

the optimisation process aims to identify the set of structural solutions that minimise the stress state and the deformation to which the analysed structure is subjected while respecting the required constraints. To this end, a Matlab framework is defined to optimise the secondary mirror. The algorithm is based on the results of FEM analyses; therefore, it is possible to prove the results using common engineering methods. The constraints on the plate deformation are based on previous studies [17,18], while the maximum allowable stress is set based on the engineering sense given the material of brackets and plate, and that the components must withstand cyclic loads (wind and temperature) and to avoid yielding. The maximum stress can be compared, for each configuration, to the fatigue limit of the components given that they are subjected to two alternate loads, i.e., wind and temperature, and to a constant load, i.e., the weight.

Optimisation Algorithm

In a generic optimisation process, the following entities are identified:

- Design variables: These are the quantities whose values are modified in the optimisation process to determine the optimal solution to the problem. These variables can be discrete or vary within a continuous range of values.
- Objective function: The objective function is the function that the optimiser aims to minimise (or maximise). It depends on the values of the design variables. In the case where more than one objective function is considered within the optimisation process, it is referred to as multi-objective optimisation.
- Constraints: Constraints represent conditions that limit the search space for the optimal solution. They are expressed in the form of equations and/or inequalities, generally as a function of constant parameters, design variables, and/or the objective function.

In this work, the identified design variables are the bracket (i) number, (ii) height, and (iii) thickness, as well as (iv) plate thickness, as reported in Table 2. The number of brackets can only take integer values, while, for the other variables, it has been assumed that the same holds to reduce the computational load caused by a large number of combinations and to obtain standard values for the implementation phase of the proposed design solution. The implemented algorithm, which is shown in Figure 9, is used to check whether the configurations satisfy the imposed constraints or not, and it consists of the following steps:

- The amplification of the stress state is carried out according to the coefficients defined in Eurocode 3 [19], specifically $c_{weight} = 1.4$ for the stresses caused by the weight force and $c_{wind} = 1.5$ for those due to wind action.
- Sum of the stress state obtained in the different loading conditions for all the components. Given the two conditions for the wind, two different summation terms will be obtained, one for the medium wind condition and one for the maximum wind condition.
- Sum of plate displacements under the different loads. Given the two conditions for the wind, two different summation terms will be obtained, one for the medium wind condition and one for the maximum wind condition.
- Evaluation of the slope deviation [17,18], that is, the angle between the actual and ideal mirror surface normal.
- For each configuration, check that
  - Maximum stress $\sigma_{max} \leq 80$ MPa for each component. This constraint is used to minimise fatigue damage to the components since the wind and the temperature are cyclic loads and, at the same time, to avoid welding.
  - Plate slope deviation $SD_{rms} \leq 1$ mrad, to minimise beam quality loss and pointing errors.
  - Plate relative displacement $u_{rel} \leq 1$ mm, to minimise beam quality loss and pointing errors.
- If all the checks are satisfied, then the configuration is approved by the algorithm and the weld assessment is performed; otherwise, it is rejected.

The optimisation algorithm is used to check whether the configurations satisfy the constraints or not. Then, it rejects the configurations which do not satisfy the constraints and stores the ones that satisfy them. In this way, it is possible to automatically select the optimal configurations.

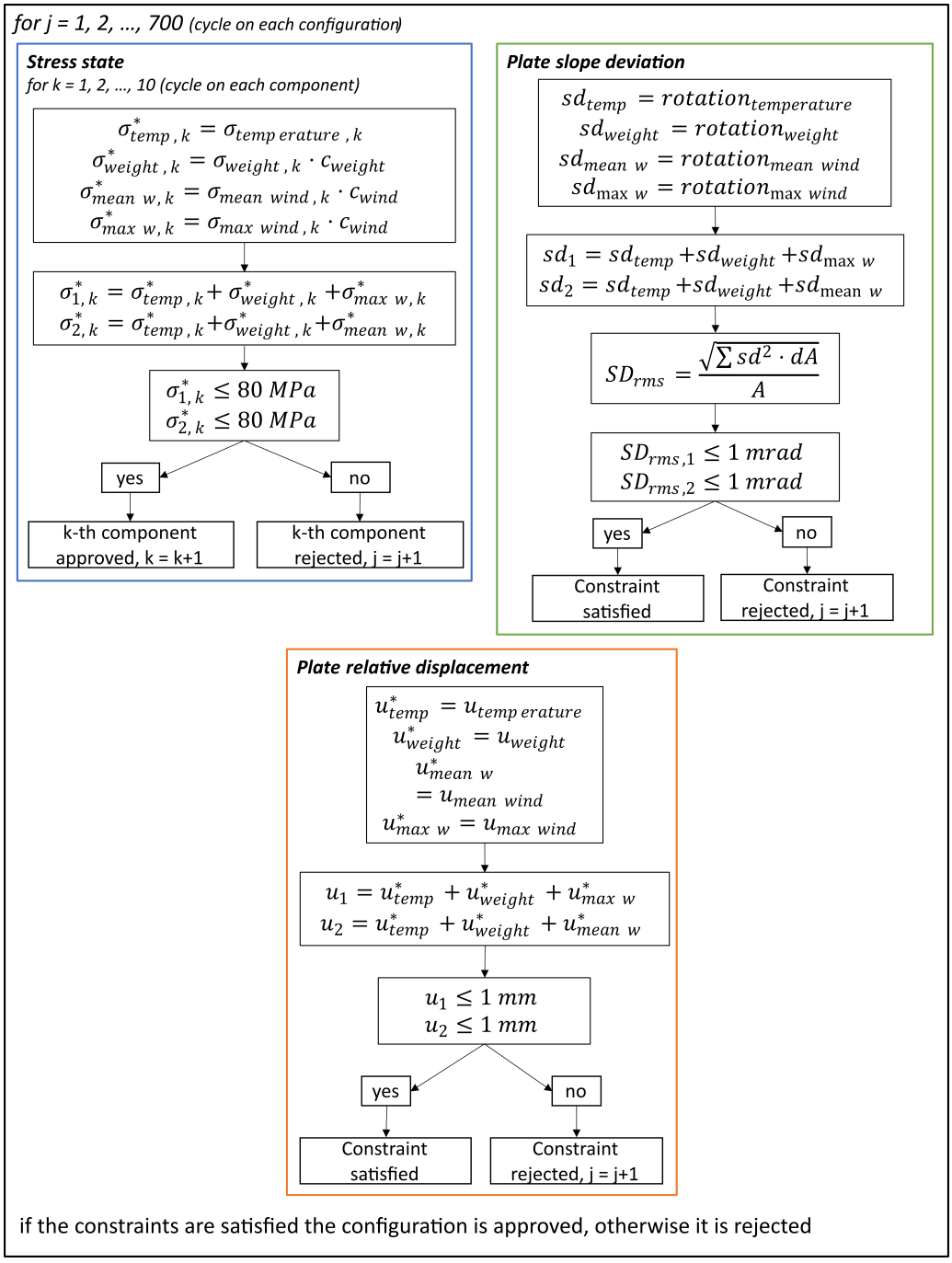


**Figure 9.** Pseudo code of the implemented optimisation algorithm.

In previous work [17,18], the plate slope deviation constraint was set separately for the coordinate directions ($x$, $y$, and, in 3D structures, $z$), according to Equations (1) and (2) (only the $x$-direction is shown since the same formula holds for the other directions). However, in this work, a cautionary approach has been implemented by using the magnitude of the total plate rotation $sd$ instead of the rotation along a specific direction $sdx$. This is carried out because the magnitude of the plate rotation is greater than the rotation of the plate along an individual direction. By doing so, it is possible to simultaneously and conservatively

satisfy the constraint on both the $x$ and $y$ direction by imposing that the maximum value of the overall slope deviation $SD_{rms}$ is less than 1 mrad.

$$sdx = \left(\frac{d}{dx}z\right)_{computed} - \left(\frac{d}{dx}z\right)_{ideal} \quad (1)$$

$$SDx_{rms} = \frac{1}{\sqrt{A}}\sqrt{\iint sdx^2 dxdy} \quad (2)$$

The weld assessment is performed according to Eurocode 3 [19] under the hypothesis that the weld has length and thickness equal to the smaller thickness between the plate and the brackets.

The implemented algorithm extracts the results of FEM simulations (stress state, and deformation and displacement fields). Therefore, it does not have information about the geometry of the problem with the exception only of the number of brackets. The maximum allowable stress is based on the steel used to avoid fatigue-related issues during operations since both the wind and temperature to which the mirrors are subjected fluctuate during each day. Moreover, taking into account that the constraints on the plate deformation (i.e., the slope deviation and plate relative displacement) are set to avoid loss in the reflected beam quality and pointing errors the algorithm can be easily used or adapted to the structural optimisation of other types of mirrors or components for CSP plants. Moreover, the proposed algorithm allows for identifying those configurations which satisfy the imposed structural constraints (i.e., stress state, slope deviation, and relative displacement) obtaining a set of optimal solutions from the structural point of view among the explored variability range of the parameters under optimisation. Eventually, among the identified solutions, it is possible to choose the best solution from a manufacturing point of view. For example, the optimisation of the structure weldability can be carried out by selecting the configuration in which the plate and brackets have the same thickness.

## 3. Results

The results of the proposed framework are presented in this section. The optimisation algorithm outputs four possible configurations, that are reported in Table 3. The "Configuration Name" reported in the table gives the design variable values used for each configuration: the first number refers to the number of the "C" shaped bracket, the second to the bracket thickness (TC), the third to the bracket height (HC), and the last one to the plate thickness (TP). By looking at the four configurations selected by the algorithm, it is possible to notice that there are optimal values for both bracket thickness and height, which are 3 mm and 200 mm, respectively. Instead, the minimum plate thickness allowable is found to be 3 mm and in correspondence with the maximum number of brackets welded on the plate (9). Therefore, the second configuration of Table 3 can be the final choice for the design of the secondary mirrors since it minimises the plate thickness among the four possible configurations and it guarantees the same thickness for the brackets and the plate itself, helping the welding process.

By looking at Figure 10 it is possible to see that the slope deviation is a very restrictive constraint, leading to the exclusion of most of the configurations since only 110 out of 700 satisfy this constraint and then only 4 out of 110 also satisfy the other constraints. In Tables 4 and 5 it is possible to see the maximum stresses acting on the plate in the selected configurations by summing the gravity, the thermal load, and either the mean wind or the maximum wind. The second configuration shown in Table 3 seems to be the best one by looking at Table 4 even if the differences from the other configurations are small. For this reason, it can be more interesting to look at Table 5 since the second configuration shows the highest maximum plate stress; even if it must be stated that the condition of maximum wind speed at 30 m/s is rare, it is still to be considered.

The results of the FEM simulations are presented as an example and just for one configuration, the *C_9_TC_3_HC_200_TP_3*, i.e., the second configuration of Table 3. The results

are shown on the undeformed structure, and separately for the four loading conditions and each of the three analysed quantities: Von Mises stresses [MPa] from Figures 11–14, displacements [mm] from Figures 15–18, and rotations [rad] from Figures 19–22. From the figures, it can be noted that the "C" brackets are the most stressed components, especially around the hole for bolting to the support. However, this point does not pose particular problems since the bolting has not been modelled and the tightening of the brackets to the support prevents the intensification of stresses that occurs during the simulation, thanks to the compressive preload necessary for tightening. It is also possible to note that the most critical load condition for the stress state is the maximum wind at 30 m/s, while the weight and the temperature induce relatively low stresses in both the plate and the brackets.

The loading condition that induces the greatest displacements is due to the heating effect of the mirror at 200 °C, i.e., the thermal load. This load condition causes a uniform expansion of the plate that is constrained by the brackets. As a consequence, from Figure 16 it is possible to notice that there is a circular central region of the plate with lower displacements than the corners of the plate itself due to the arrangement of the brackets. As a consequence, the brackets placed at the corners are the ones which experience the greatest rotation that is backwards with respect to their orientation due to the plate expansion.

Instead, concerning the maximum wind condition, it can be seen in Figure 18 that the plate deformation is not uniform and this is due to the fact that the plate is oriented at 13.5° with respect to the horizontal. This behaviour is reflected by the rotation of the structure shown in Figure 22 that, as expected, is greater close to the maximum displacement region and where the brackets are welded to the plate. In general, the action of the mean wind is almost negligible for all three quantities of interest since it causes very low stresses and deformations in the structure, as it is possible to see in Figure 13, Figure 17, and Figure 21, respectively.

**Table 3.** Configurations selected by the optimisation algorithm.

| Configuration Name | #C | Bracket Thickness [mm] | Bracket Height [mm] | Plate Thickness [mm] |
|---|---|---|---|---|
| *C_8_TC_3_HC_200_TP_5* | 8 | 3 | 200 | 5 |
| *C_9_TC_3_HC_200_TP_3* | 9 | 3 | 200 | 3 |
| *C_9_TC_3_HC_200_TP_4* | 9 | 3 | 200 | 4 |
| *C_9_TC_3_HC_200_TP_5* | 9 | 3 | 200 | 5 |

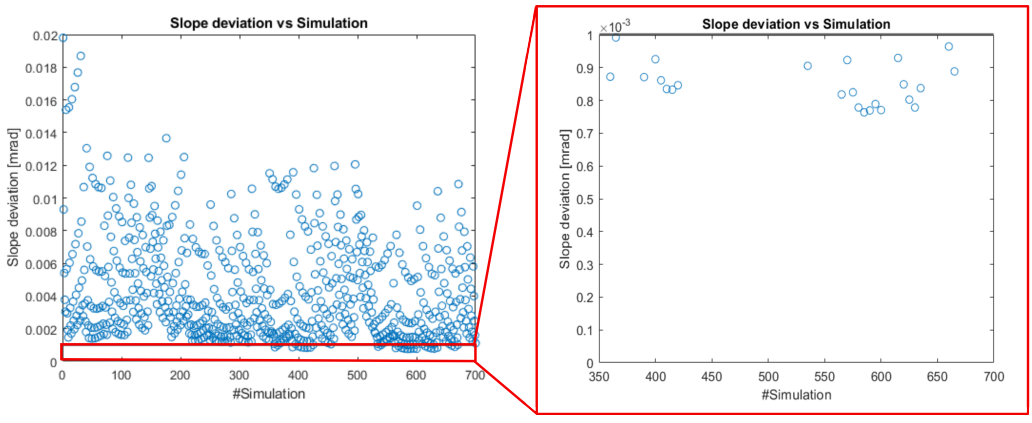


**Figure 10.** Influence of slope deviation constraint. The optimal region is highlighted in red.

**Table 4.** Maximum plate stress obtained by summing the contributions of weight, temperature, and mean wind for the four configurations selected by the algorithm.

| Configuration Name | Max Stress [MPa] |
|---|---|
| *C_8_TC_3_HC_200_TP_5* | 29.16 |
| *C_9_TC_3_HC_200_TP_3* | 26.80 |
| *C_9_TC_3_HC_200_TP_4* | 29.09 |
| *C_9_TC_3_HC_200_TP_5* | 28.46 |

**Table 5.** Maximum plate stress obtained by summing the contributions of weight, temperature, and maximum wind for the four configurations selected by the algorithm.

| Configuration Name | Max Stress [MPa] |
|---|---|
| *C_8_TC_3_HC_200_TP_5* | 44.54 |
| *C_9_TC_3_HC_200_TP_3* | 55.89 |
| *C_9_TC_3_HC_200_TP_4* | 47.71 |
| *C_9_TC_3_HC_200_TP_5* | 42.77 |

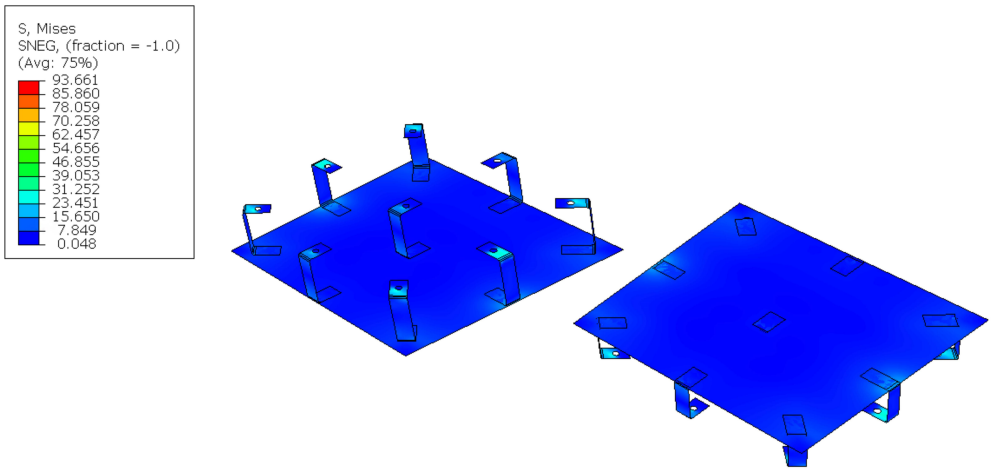


**Figure 11.** Von Mises stresses [MPa] for the secondary mirror when subjected to its weight.

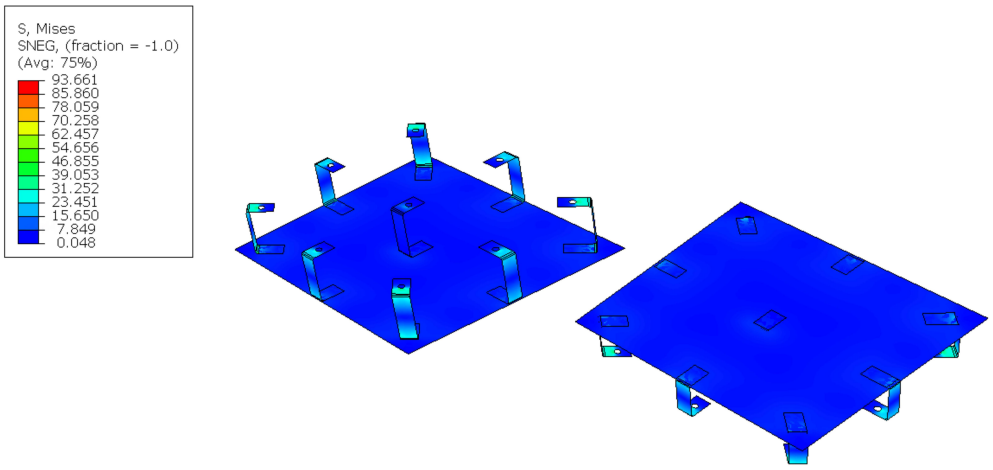


**Figure 12.** Von Mises stresses [MPa] for the secondary mirror when subjected to the thermal load.

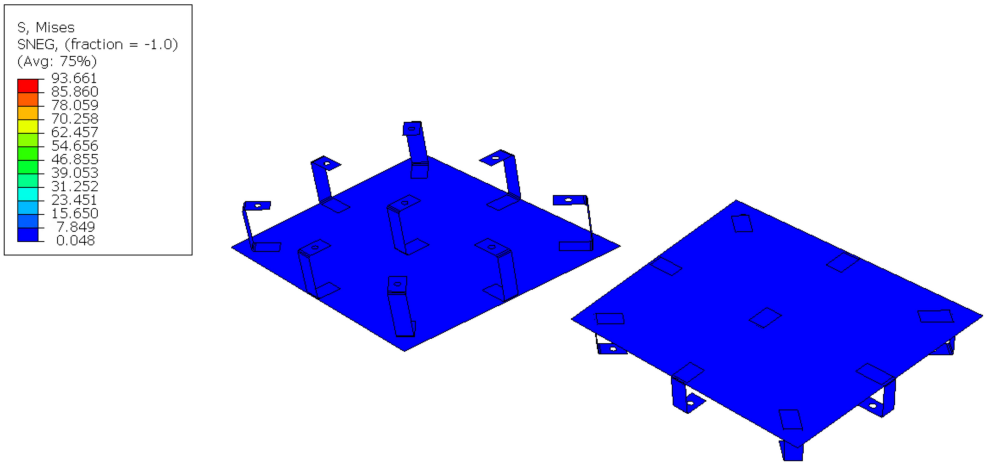


**Figure 13.** Von Mises stresses [MPa] for the secondary mirror when subjected to the operative wind (13 km/h).

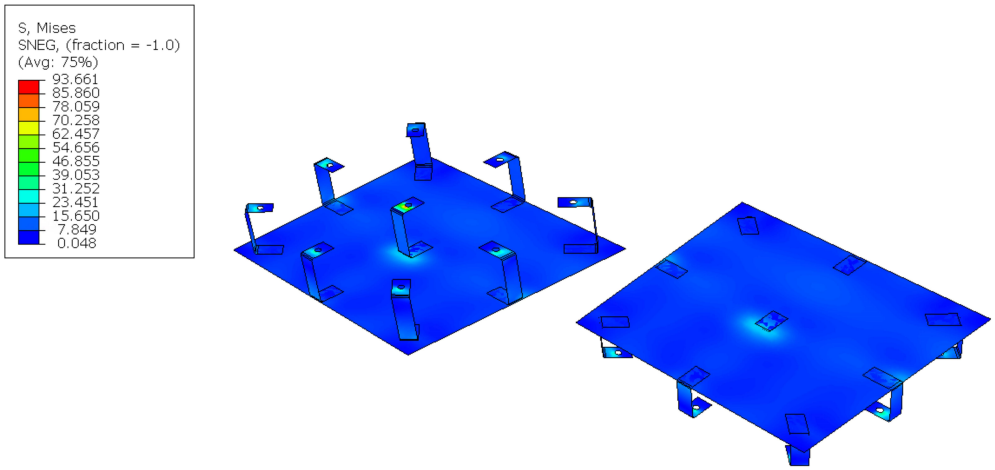


**Figure 14.** Von Mises stresses [MPa] for the secondary mirror when subjected to the maximum wind (30 m/s).

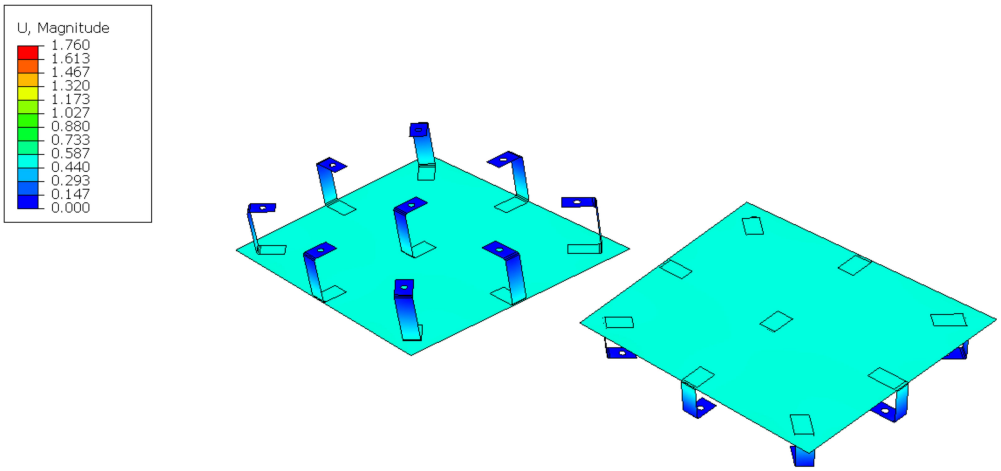


**Figure 15.** Displacement[mm] for the secondary mirror when subjected to its weight.

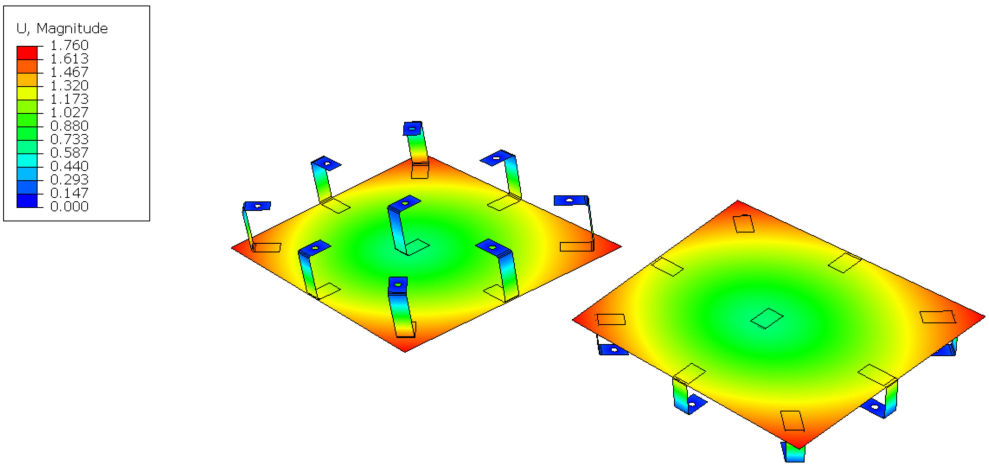


**Figure 16.** Displacement[mm] for the secondary mirror when subjected to the thermal load.

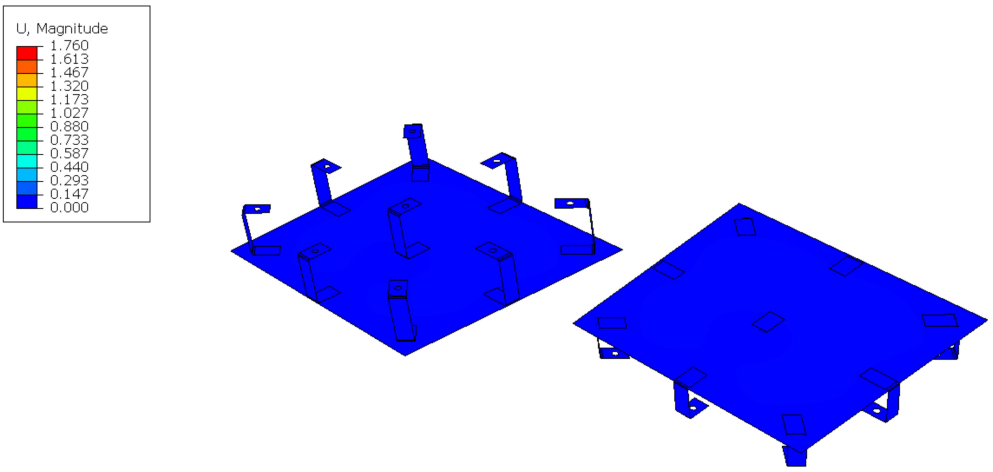


**Figure 17.** Displacement[mm] for the secondary mirror when subjected to the operative wind (13 km/h).

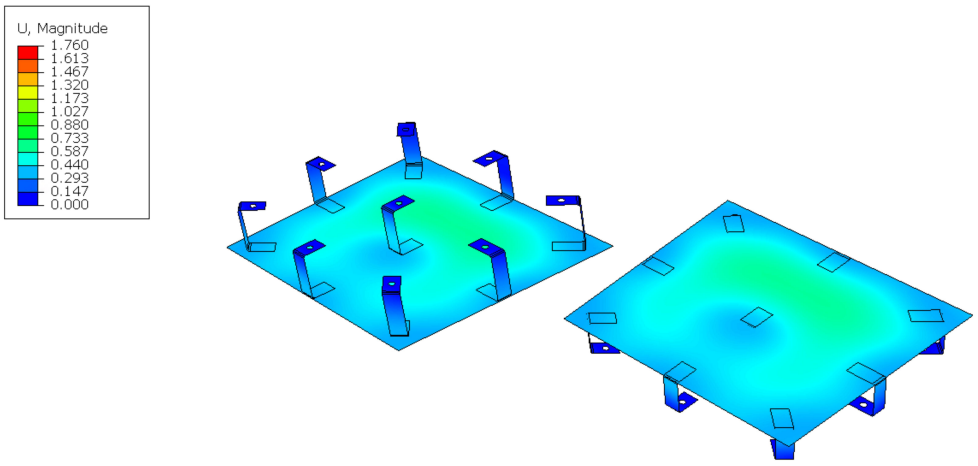


**Figure 18.** Displacement[mm] for the secondary mirror when subjected to the maximum wind (30 m/s).

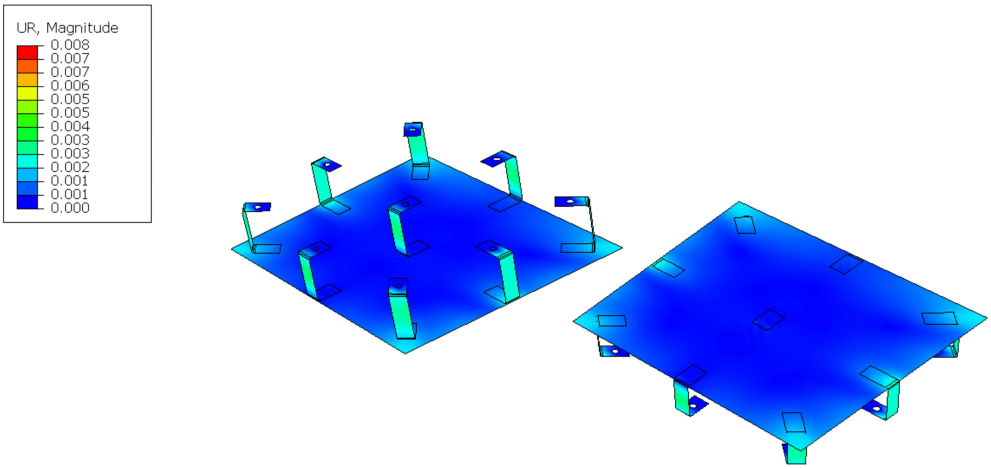


**Figure 19.** Rotation[rad] for the secondary mirror when subjected to its weight.

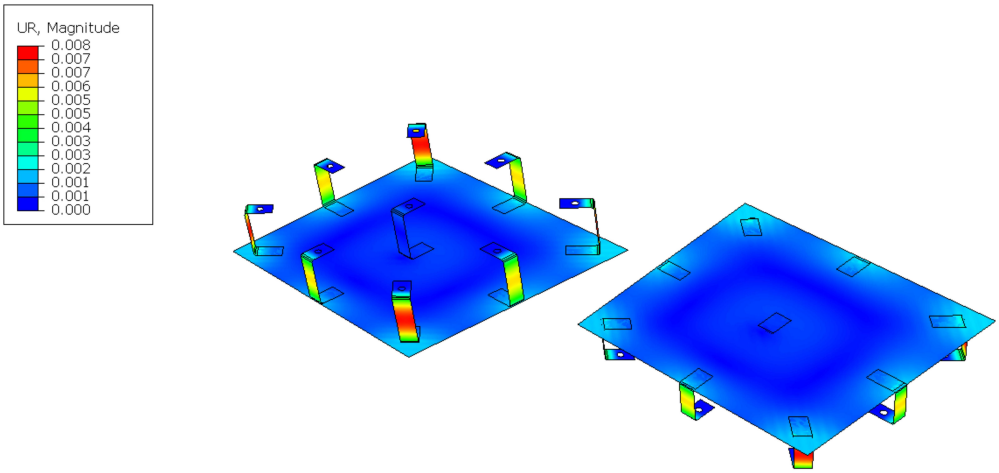


**Figure 20.** Rotation[rad] for the secondary mirror when subjected to the thermal load.

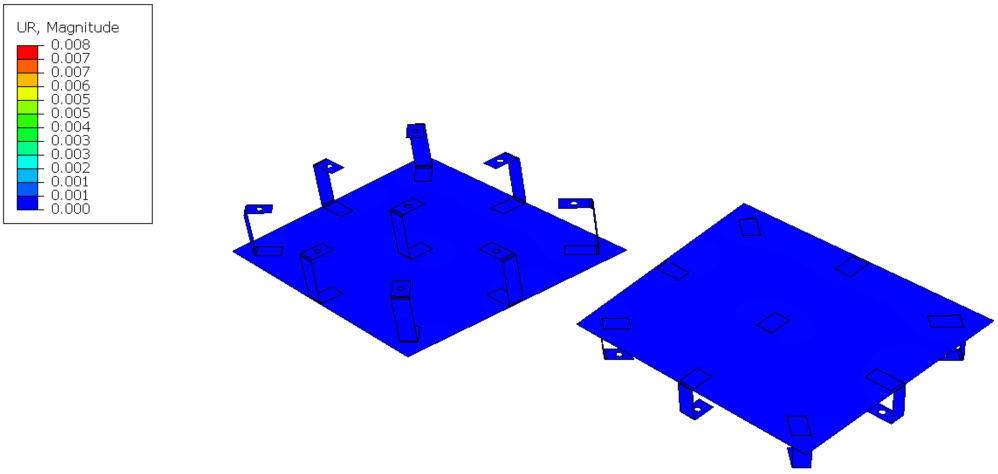


**Figure 21.** Rotation[rad] for the secondary mirror when subjected to the operative wind (13 km/h).

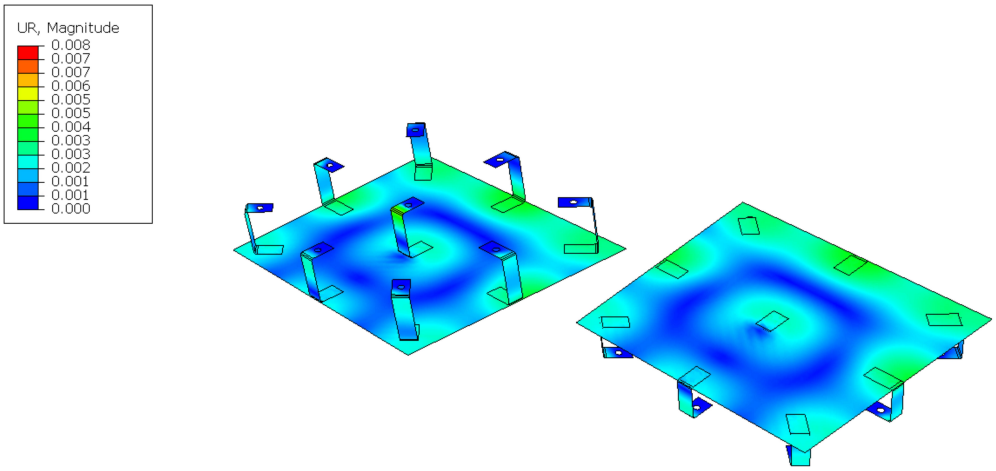


**Figure 22.** Rotation[rad] for the secondary mirror when subjected to the maximum wind (30 m/s).

## 4. Discussion

The structural model, implemented in Abaqus, allows the evaluation of several indicators of structural and optical performance related to the adopted configuration, such as deformation (rotation), displacements, and stress state generated by the applied loads. The optimisation algorithm processes these indicators to evaluate the performances of the configurations analysed; in particular, the optical efficiency is optimised by exploiting the constraint on the slope deviation, which is a measure of the plate deformation. The structural resistance is evaluated by imposing a limit on the maximum allowable strength.

The results showed that the optimal configurations are the ones with the highest number of brackets, 8 and 9, and with the highest plate thicknesses, from 3 mm to 5 mm, but there is not a clear optimum between these configurations. On the contrary, optimal values for the bracket thickness and height have been found and are 3 mm and 200 mm, respectively. However, even if there is no clear optimal configuration, some considerations can be made since using the plate with a thickness of 3 mm allows the welding of components with the same thickness. In addition, it helps reduce the weight and cost of the structure with respect to the other configurations with nine brackets. Therefore, the final choice can be the only configuration with 3 mm thickness for both plate and brackets, that is the *C_9_TC_3_HC_200_TP_3*.

Further investigations can be conducted by decreasing the increment for the thicknesses and for the height, as well as extending the bracket height range. Using a thinner plate and thinner brackets, as well as brackets with a lower height allows for a relevant cost and weight reduction on the entire plant, which is a desirable feature. The choice of the final design can not be made without considering also the optical efficiency in the deformed condition of the secondary mirror, even if this is preliminarily made by imposing a constraint on the slope deviation in the optimisation algorithm.

## 5. Conclusions

This study describes the framework developed to conduct the structural optimisation of the design of secondary mirrors for a CSP plant, which consists of the mirror itself and the brackets that allow it to be fixed to the supports. The framework exploits Python code used to modify the structural model developed in Abaqus according to the different configurations and to run the FEM analysis in the four loading conditions analysed. Then, the simulation results are processed in Matlab to check whether the configurations analysed satisfy the constraints imposed for structural and optical efficiency purposes. The outcomes of the study are:

- The optimisation procedure outputs only 4 of the analysed 700 configurations.
- Optimal values for bracket thickness and height have been found, corresponding to 3 mm and 200 mm, respectively.

- Only one configuration uses eight brackets and this implies the maximum plate thickness, i.e., 5 mm.
- Three configurations have nine brackets and the plate thickness is respectively 3 mm, 4 mm, and 5 mm.
- Thus, the configuration *C_9_TC_3_HC_200_TP_3* could be selected as optimal since it also helps the welding of the brackets on the plate thanks to the same 3 mm thickness between the brackets and the plate.

The tools implemented in the environment described in this study have strong development potential. For example, the optimisation algorithm is flexible and capable of handling a process based on the satisfaction of an unlimited number of constraints. With this perspective, new constraints could be added or the algorithm could be adapted to new case studies. For instance, a similar methodology could be coupled with a ray-trace solver and thermo-economic model to evaluate the impact of costs of secondary mirrors on overall plant LCOH. Furthermore, it is possible to consider integrating the structural model implemented in Abaqus by adding design variables, moving towards a more comprehensive but computationally expensive optimisation process. Finally, to limit the computational resources required to manage a heterogeneous computing environment, which combines a part of the algorithm implemented in Abaqus (the structural model) and a part in Matlab (the optimisation algorithm), porting the entire environment to a single platform is identified as a possible future development. This practice would allow both using the computing environment to conduct sensitivity analyses, important for identifying the design variables that most influence the optimisation process, and incorporating more advanced concepts related to structural analysis into the optimisation phase, such as Reliability-Based Design Optimisation (RBDO).

**Author Contributions:** Conceptualization, M.C.; Methodology, L.P. and M.F.; Formal analysis, L.P. and M.F.; Writing—original draft, L.P.; Writing—review & editing, L.P. and C.B.; Visualization, R.M.; Supervision, F.C. and F.B.; Project administration, M.G. All authors have read and agreed to the published version of the manuscript.

**Funding:** This work is part of the Research and Innovation Project "Solargrid: Sistemi sOlari termodinamici e fotovoLtaici con Accumulo peR co-GeneRazIone e flessibilità Di rete"—cod. ARS01_00532. The project has been jointly funded by the European Union and the Italian Research and University Ministry (MIUR) under the Programma Operativo Nazionale "Ricerca e Innovazione" 2014–2020 (PON "R&I" 2014–2020).

**Data Availability Statement:** No new data were created or analyzed in this study. Data sharing is not applicable to this article.

**Acknowledgments:** The support of all the R&D Magaldi team in the design of a secondary mirror for the beam-down of the CSP Magaldi technology is gratefully acknowledged.

**Conflicts of Interest:** The authors declare no conflict of interest. The funders had no role in the design of the study; in the collection, analyses, or interpretation of data; in the writing of the manuscript; or in the decision to publish the results.

## References

1. Haghghi, M.A.; Holagh, S.G.; Chitsaz, A.; Parham, K. Thermodynamic assessment of a novel multi-generation solid oxide fuel cell-based system for production of electrical power, cooling, fresh water, and hydrogen. *Energy Convers. Manag.* **2019**, *197*, 111895. [CrossRef]
2. Almatrafi, E.; Khaliq, A.; Kumar, R.; Bamasag, A.; Siddiqui, M.E. Proposal and Investigation of a New Tower Solar Collector-Based Trigeneration Energy System. *Sustainability* **2023**, *15*, 7474. [CrossRef]
3. Gledhill, S.; Hildebrandt, C.; Uhlig, R.; Wette, J.; Sutter, F. Secondary reflector tested at high temperatures and high radiation intensities. In Proceedings of the International Conference on Concentrating Solar Power and Chemical Energy Systems (SolarPACES) 2021, Online, 27 September–1 October 2021. [CrossRef]
4. Fernandez-Garcia, A.; Cantos-Soto, M.E.; Roger, M.; Wieckert, C.; Hutter, C.; Martinez-Arcos, L. Durability of solar reflector materials for secondary concentrators used in CSP systems. *Sol. Energy Mater. Sol. Cells* **2014**, *130*, 51–63. [CrossRef]

5. Siddiqui, M.E.; Almitani, K.H. Energy and Exergy Assessment of S-CO2 Brayton Cycle Coupled with a Solar Tower System. *Processes* **2020**, *8*, 1264. [CrossRef]
6. German Aerospace Center (DLR) Institute of Solar Research. Solar Thermal Power Plants. 2021. Available online: https://www.solarpaces.org/wp-content/uploads/Study_Solar_thermal_power_plants_DLR_2021-05.pdf (accessed on 15 May 2023).
7. Ben-Zvi, R.; Segal, A.; Epstein, M. Beam-Down Mirror: Thermal and Stress Analyses. *J. Sol. Energy Eng.* **2009**, *131*, 041003. [CrossRef]
8. Zanut, A.; Binotti, M.; Giostri, A. Design and Optimization of a Point Focus Beam-Down System. Master's Thesis, PoliMi, Milano, Italy, 2021.
9. Calvet, N.; Slocum, A.H.; Gil, A.; Grange, B.; Lahlou, R.; Hamer, T.T.; Diago, M.; Tetreault-Friend, M.; Codd, D.S.; Trumper, D.L.; et al. Dispatchable Solar Power Using Molten Salt Directly Irradiated from Above. *Sol. Energy* **2021**, *220*, 217–229. [CrossRef]
10. Diago, M.; Calvet, N.; Armstrong, P.R. Net power maximization from a faceted beam-down solar concentrator. *Sol. Energy* **2020**, *204*, 476–488. [CrossRef]
11. Chirone, R.; Salatino, P.; Ammendola, P.; Solimene, R.; Magaldi, M.; Sorrenti, R.; Michele, G.D.; Donatini, F. Development of a Novel Concept of Solar Receiver/Thermal Energy Storage System Based on Compartmented Dense Gas Fluidized Beds. Engineering Conferences International. 2013. Available online: https://dc.engconfintl.org/fluidization_xiv/123 (accessed on 15 May 2023).
12. Lahlou, R.; Armstrong, P.R.; Calvet, N.; Slocum, A.H.; Shamim, T. Testing of a secondary concentrator integrated with a beam-down tower system under non-liquid cooling strategies. In Proceedings of the SolarPACES 2017: International Conference on Concentrating Solar Power and Chemical Energy Systems, Santiago, Chile, 26–29 September 2017. [CrossRef]
13. Wang, S.; Asselineau, C.A.; Fontalvo, A.; Wang, Y.; Logie, W.; Pye, J.; Coventry, J. Co-optimisation of the heliostat field and receiver for concentrated solar power plants. *Appl. Energy* **2023**, *348*, 121513. [CrossRef]
14. Jafrancesco, D.;Sansoni, P.; Francini, F.; Fontani, D. Strategy and criteria to optically design a solar concentration plant. *Renew. Sustain. Energy Rev.* **2016**, *60*, 1066–1073. [CrossRef]
15. Diaz-Heras, M.; Moya, J.D.; Belmonte, J.F.; Corcoles-Tendero, J.I.; Molina, A.E.; Almendros-Ibanez, J.A. CSP on fluidized particles with a beam-down reflector: Comparative study of different fluidization technologies. *Sol. Energy* **2020**, *200*, 76–88. [CrossRef]
16. Diaz-Heras, M.; Barreneche, C.; Belmonte, J.F.; Calderon, A.; Fernandez, A.I; Almendros-Ibáñez, J.A. Experimental study of different materials in fluidized beds with a beam-down solar reflector for CSP applications. *Sol. Energy* **2020**, *211*, 683–699. [CrossRef]
17. Röger, M. Heliostat Performance Testing Guideline—Status Update in SolarPaces Task III Workshop. Santiago de Chile, 25 September 2017. Available online: https://elib.dlr.de/115415/ (accessed on 16 May 2023).
18. Solar Paces Task III Measurement Of Solar Weighted Reflectance Of Mirror Materials For Concentrating Solar Powertechnology With Commercially Available Instrumentation. Available online: http://www.solarpaces.org/Tasks/Task3/Interim_Reflectance_Guideline.pdf (accessed on 16 May 2023).
19. EN 1993-1-1:2005 +A1:2014. Eurocode 3: Design of Steel Structures. Available online: https://eurocodes.jrc.ec.europa.eu/EN-Eurocodes/eurocode-3-design-steel-structures (accessed on 14 April 2023).